TWMS J. App. Eng. Math. V.1, N.1, 2011, pp. 1-26

COMPUTATIONAL AND ASYMPTOTIC METHODS IN AEROACOUSTICS WITH APPLICATIONS

C. F. DELALE[1], B. ZAFER[2] AND A. R. ASLAN[2] §

Abstract. In this article the computational and asymptotic methods used in aeroacoustics are reviewed. In particular, two different aeroacoustic applications are demonstrated. In the first problem we investigate the first and second order asymptotic predictions of the thickness and loading noise of a subsonic B-bladed helicopter rotor in the far field and compare the SPL noise results with those of full numerical computations. The results of the second order asymptotic formula seem to be in better agreement with full numerical computations than the first order asymptotic formula. In the second problem, the effect of acoustic wave propagation in transonic nozzle flow is investigated by solving the unsteady quasi-one-dimensional transonic nozzle equations in conservative form using high order computational aeroacoustic schemes, where a novel non-reflecting boundary condition is implemented in addition to the standard non-reflecting boundary condition using characteristics. Excellent agreement with the exact solution is obtained in each case.

Keywords: Aeroacoustics, Acoustic Analogy, Helicopter Rotor Noise, Acoustic Disturbances, Transonic Nozzle Flows.

AMS Subject Classification: 65M06, 65M80, 76H05, 76N15, 76Q05

1. Introduction

Aeroacoustics is concerned with sound, generated by turbulent fluid motion or aerodynamic forces interacting with surfaces as mentioned before. Governing equations of gas dynamics (e.g. the Navier-Stokes equations) describe the motion in a fluid. Hence, the solution of these equations, subjected to boundary conditions, will include not only convection and diffusion, but also acoustic wave propagation. The acoustic part of the solution can not, in general, be separated from the rest of the solution. However, in many solution methods such as acoustic analogy and numerical prediction methods, the flow and the acoustics are assumed as two different fields. Aeroacoustics is a relatively new research area which began about fifty years ago. It was developed in order to investigate the reduction of aircraft noise levels. In the beginning, jet noise was the most important

[1] Department of Mechanical Engineering, Işık University, 34980 Şile, Istanbul, Turkey,
e-mail: delale@isikun.edu.tr

[2] Faculty of Aeronautics and Astronautics, Istanbul Technical University, 34469 Maslak, Istanbul, Turkey,
e-mail: zaferba@itu.edu.tr and aslanr@itu.edu.tr

§ Manuscript received 1 May 2011.

noise source because of the use of aircraft turbojet engines. During the three decades between 1960 and 1990, rotating blades of machinery became a significant source because of the development of turboshaft engines. The field of aeroacoustics can be classified as free space domain problems (e.g. jet noise), free space domain problems with solid surfaces (e.g. helicopter rotors and propellers) and bounded domain problems (e.g. ducted fans). In free space problems with solid surfaces, noise has been an undesirable phenomenon of aerospace vehicles since the early years of propulsion. For instance, the operating environment of a helicopter rotor is extremely complex and fundamentally unsteady [1]. The various types of helicopter noise contribute to both discrete frequency and broadband noise generation through several distinct noise mechanisms. Thickness noise and loading noise, known together as rotational noise, are related to linear aerodynamic theory. In this theory quadrupole effects can be neglected completely. Thickness noise is due to the displacement of the fluid in the flow field by the rotor blade, and loading noise is caused by the accelerating force on the fluid generated by the moving blade surface. Blade-Vortex Interaction noise (BVI) occurs as a result of the tip vortex interacting with the blade. At high advancing tip speeds, the rotor generates impulsive noise of high intensity, called High Speed Impulsive noise (HSI). Essentially all broadband noise is generated by random loading on the rotor blade. Broadband noise can be generated by turbulence phenomena associated with the flow near or on the blade surface that is usually called turbulence noise [1]. In order to understand the more recent advances in helicopter noise prediction, it is helpful to go back to the late 1930s. The earliest methods used a point force model of the propeller for noise prediction. The first successful prediction theory was developed by Gutin [2] and the first theoretical result was obtained by using a stationary oscillating point force for calculating the first few harmonics of propeller noise due to blade loads. Later a thickness source was added. Ernsthausen in Germany [3] and Deming in the U.S. [4] recognized the importance of finite blade thickness. Garrick and Watkins [5] extended Gutin's result to propellers in forward flight in the early fifties. In the mid-fifties, Arnoldi [6] obtained an expression for thickness noise in the frequency domain. All of the early studies investigated only propeller noise. In 1952, Lighthill [7] introduced the acoustic analogy. Lighthill proposed a methodology for the prediction of aerodynamic noise. He suggested that in the neighborhood of a source, space can be divided into two regions. Noise is generated in the near vicinity of the source, called compact source region, which has a relatively small space extent. Then the generated acoustic waves propagate linearly through the undisturbed medium, called the propagation region. Lighthill introduced this space splitting into the conservation equations of fluid dynamics and derived the so-called Lighthil's acoustic analogy. The major significance of Lighthill's acoustic analogy is that sound generated aerodynamically is computed based on aerodynamical data obtained from Computational Fluid Dynamics (CFD). Since Lighthill's acoustic analogy is based on the conservation laws and no simplifications are made during the derivation, the analogy is valid for all flows without limitation [8]. In the 1960's, the noise of helicopters became an important issue. Initially both the piston engine and the rotor were the major generators of noise, but with the introduction of the turboshaft engine, the main and tail rotors became the dominant external noise sources because of the high speed of the rotors. Some of the first noise prediction theories applied specifically to helicopter rotors were developed by Lowson [9] and Wright [10]. Lowson arrived at a simple, but powerful expression

for a moving point source. At this time, the development of high speed digital computers helped the researcher to use more realistic models in their study. For instance, Lowson and Ollerhead [11] developed a computer code for rotor noise prediction. Considerable experimental and theoretical studies have been carried out to understand the source mechanisms of helicopter rotors. In 1969, Ffowcs Williams and Hawkings (FW-H) published their now classic paper "Sound Generation by Turbulence and Surfaces in Arbitrary Motion" [12], which generalized Lighthill's acoustic analogy [7] to include the effects of general types of surfaces and motions. Using the mathematical theory of distributions (also known as generalized functions), they were able to rearrange the Navier-Stokes equations into the form of an inhomogeneous wave equation with a quadrupole source distribution in the volume surrounding the body and monopole and dipole sources on the body surface. Ffowcs Williams and Hawkings paper encouraged theoretical work on helicopter rotor noise in the 1970's. Hawkings and Lowson [13] and Farassat [14,15] applied the FW-H equation to the problem of rotor noise prediction. At this time acoustic code prediction development was limited by the lack of aerodynamic theories which were not sophisticated enough to satisfy the input requirements of the aeroacoustic codes. The insight into noise generation aspect of high speed propeller was given by Yu [16] which was an extended version of the study of Hawkings and Lowson [13] in forward flight. Also in the same period, Hanson [17,18] had successfully adapted his frequency domain method to aeroacoustic design of high speed propellers. By the 1980's, theoretical development in aeroacoustics became more complicated. Several model scale and flight tests were carried out to understand and classify the physical sources of helicopter rotor noise. For instance, NASA/AHS Rotorcraft Noise Reduction Program (NR) [19] improved experimental data and theoretical understanding of sound generation. In parallel with the NR program, there were several high quality acoustic tests conducted in the German-Dutch Wind tunnel (DNW) [20,21]. Farasat and Succi [22] predicted the transonic effects contained in the quadrupole term. Brentner [23] incorporated the Farassat and Succi formulation into NASA Langley's code, which is now called WOPWOP. This code has been used for the prediction of helicopter rotor thickness and loading noise including detailed blade motion. In 1990's, much of the research focused on the prediction of impulsive and broadband noise and the quadrupole term of the FW-H equation. Also, the Kirchhoff formulation for moving surfaces rapidly gained popularity [24], but later it was demonstrated that the FW-H equation is better than the Kirchhoff formula, especially when used with a permeable surface surrounding all the sources [25]. In order to understand impulsive noise, Brentner and Farassat [26] developed a supersonic quadrupole formulation that did not have a Doppler singularity in their formulation. Howe [27] gives a comprehensive account of rotor broadband noise prediction. Ianniello [28,29] has also developed quadrupole noise prediction codes that integrate the FW-H equation on a supersonic rotating domain. In the same time period, there has been an increased interest in the development of methods suitable for numerical simulations of unsteady wave propagation in aeroacoustics. Consequently, a new field known as computational aeroacoustics (CAA) emerged. It became an efficient tool for noise prediction that depended on high capacity and fast computer technology. Computational aeroacoustics (CAA) is mostly employed in research, in order to investigate the noise generation and propagation mechanisms in detail. The need of highly accurate numerical methods was recognized since the earliest stages of the development of CAA.

The propagation of sound waves in far-field requires long-time integration with minimal dissipation and dispersion, and this cannot be done using the numerical schemes generally used in Computational Fluid Dynamics (CFD). Therefore, new schemes with higher accuracy were proposed. Most aeroacoustics problems involve small-amplitude linear wave propagation. Today, the high order explicit Dispersion-Relation-Preserving (DRP) scheme of Tam and Webb [30] and the Optimized Compact (OC) schemes [31-35] possess the necessary accuracy and wave propagation properties for calculating linear wave propagation with minimal spatial resolution. Tam and Webb [30] presented a low dispersion scheme for the numerical solution of the linearized Euler equations. Improved dispersion characteristics in wave propagation problems were also demonstrated by Zingg [35] and Haras and Taasan [32] who optimized high-order, centered, finite-difference schemes. Low dispersion and dissipation criteria necessary for aeroacoustics computations are also fulfilled by the fourth-order accurate in space predictor corrector-type scheme, known as the 2-4 MacCormack scheme [36]. Finally, time integration was also optimized for noise computation, and low-dissipation and low-dispersion. Later the Adams-Bashforth [30] and Runge-Kutta algorithms [37-39] were constructed. Detailed comparison of advantages and disadvantages of other schemes can be found in CAA review articles by Tam [40,41], Colonius and Lele [42], Wells and Renaut [43] and Wang et al. [44].

In this investigation two different aeroacoustic problems are considered. In the first problem, propeller noise is investigated using the Green's function solution of the FW-H equation. We neglect the quadrupole term and use the frequency domain solution given by Hanson[18] using helicoidal coordinates to represent the thickness and loading source terms for subsonic flow. In this study we investigate the first and second order asymptotic predictions [45-47] in the far field, as well as the full numerical computations, for the thickness and loading noise of a subsonic B-bladed helicopter rotor. In particular we obtain the first and second order asymptotic formulas using the Debye approximation for Bessel functions of high order and evaluating the resulting integral by Laplace's method [48,49]. A 3D compressible CFD code is used to compute the aerodynamic loading on the straight rectangular blade of a 4-bladed helicopter rotor in hover. The SPL noise is then calculated by the first and second order asymptotic formulas and by full numerical computations taking into account the loading and thickness contributions. The differences in the SPL noise seem to increase with increasing Mach number, with the second order asymptotics being in much better agreement than the first order in comparison with the full numerical computations. In the second problem, the capabilities of the implementation of high order computational aeroacoustic schemes are investigated for a NASA benchmark problem [50]. In this problem the effect of acoustic wave propagation in transonic nozzle flow is investigated by solving the unsteady quasi-one-dimensional transonic nozzle equations in conservative form using high order computational aeroacoustic schemes, namely the Dispersion Relation Preserving (DRP) scheme of Tam and Webb [30] and the Optimized Compact (OC) scheme of Kim and Lee [33]. For the initial distribution we use the classical quasi-one-dimensional steady-state nozzle flow solution. In addition, we use two different nonreflecting boundary conditions, namely the well-known standard nonreflecting boundary condition of Thompson [51] and a novel one, called random nonreflecting boundary condition. Both nonreflecting boundary conditions are implemented in the two computational aeroacoustic schemes used (DRP and OC). The numerical results obtained

for each scheme are then compared against those obtained by the exact solution of the unsteady quasi-one-dimensional linearized nozzle flow equations. In particular, the exact and computed maximum pressure envelope and time-dependent pressure distributions show very good agreement.

2. The Acoustic Analogy: The Lighthill and Ffowcs Williams-Hawkings Equations

The acoustic analogy was introduced into aeroacoustics by Lighthill [7] to predict the noise generated by the jet of an aircraft turbojet engine. In this work acoustic radiation from relatively small regions of turbulent flow was calculated in an otherwise quiescent medium in which the speed of sound is c_0, the density is ρ_0 and the pressure is p_0. It was shown that, away from the compact turbulent flow region, the propagation of small pressure or density disturbances was governed by an inhomogeneous wave equation. For the derivation of Lighthill's equation, we let the acoustic density (small perturbation) be defined by $\rho' = \rho - \rho_0$ and the acoustic pressure be given by $p' = p - p_0$, where ρ and p, respectively, define the density and pressure. In particular, they are related by $p' = c_0^2\,\rho'$. The continuity and momentum equations then become

$$\frac{\partial \rho'}{\partial t} \,+\, \frac{\partial}{\partial x_i}\,(\rho u_i) \,=\, 0\,, \tag{2.1}$$

$$\frac{\partial \rho u_i}{\partial t} \,+\, \frac{\partial}{\partial x_j}\,(\rho u_i u_j) \,+\, \frac{\partial P_{ij}}{\partial x_j} \,=\, 0 \tag{2.2}$$

where u_i denote the i-th component of the velocity field, P_{ij} denotes the ij-th component of the compressible stress tensor ($P_{ij} = p\delta_{ij} - e_{ij}$, with e_{ij} denoting the ij-th components of the viscous stress tensor, for the Navier-Stokes equations and $P_{ij} = p\delta_{ij}$ for the inviscid Euler equations, where δ_{ij} denotes the ij-th component of the Kroneckar delta), x_i denotes the i-th component of the spatial coordinates and t denotes the time. By taking $\partial/\partial t$ of eq. (2.1) and $\partial/\partial x_i$ of eq. (2.2) and subtracting the latter operation from the former operation, we obtain

$$\frac{\partial^2 \rho'}{\partial t^2} \,=\, \frac{\partial^2}{\partial x_i x_j}\,(\rho u_i u_j \,+\, P_{ij}). \tag{2.3}$$

If we now write $p' = c_0^2\,\rho'$ and subtract $\nabla^2 p'$, we obtain Lighthill's equation of acoustic analogy as

$$\frac{1}{c_0^2}\,\frac{\partial^2 p'}{\partial t^2} \,-\, \nabla^2 p' \,=\, \frac{\partial^2}{\partial x_i x_j}\,(T_{ij}) \tag{2.4}$$

where T_{ij} denote the components of the Lighthill stress tensor and are given by

$$T_{ij} \,=\, \rho u_i u_j \,+\, P_{ij} \,-\, c_0^2\,\rho'\,\delta_{ij}\,. \tag{2.5}$$

It is important to note that the source term in eq. (2.4) can be shown to be of quadrupole type in an otherwise quiescent medium. Its evaluation requires knowledge of the complete flow field inside the compact region, which presumably is obtained by CFD methods. We also note that in the far field the Lighthill stress tensor T_{ij} vanishes and eq. (2.4) reduces to the classical homogeneous wave equation whose solution is readily available.
Lighthill's equation (2.4) contains only contributions from volumetric flow-induced noise sources and has to be modified when sound is generated by moving, impenetrable surfaces.

An equation in this direction has been derived by Ffowcs Willams and Hawkings [12]. We let $f(x,t) = 0$ describe a moving, impenetrable surface of a body such that $f > 0$ characterizes outside the body and $\mathbf{n} = \nabla f/|\nabla f|$ denote the unit outward normal to the surface. We also assume that the fluid is at rest in the interior of the body ($f < 0$) so that we introduce an artificial discontinuity at the surface of the body ($f = 0$). Because of this artificial discontinuity, we must modify the continuity and momentum equations as

$$\frac{\partial \rho'}{\partial t} + \frac{\partial}{\partial x_i}(\rho u_i) = \rho_0 v_n \delta(f), \tag{2.6}$$

$$\frac{\partial \rho u_i}{\partial t} + \frac{\partial}{\partial x_j}(\rho u_i u_j) + \frac{\partial P_{ij}}{\partial x_j} = l_i \delta(f) \tag{2.7}$$

where all partial derivatives are now to be understood as generalized derivatives and $\delta(f)$ is the Dirac delta distribution of f, with $v_n = \partial f/\partial t$ denoting the local normal velocity of the surface $f = 0$ and $l_i = P_{ij} n_j$ denoting the components of the local force intensity (force per unit area) that acts on the fluid. If we now take $\partial/\partial t$ of eq. (2.6) and $\partial/\partial x_i$ of eq. (2.7) and subtract one from the other, we obtain

$$\frac{\partial^2 \rho'}{\partial t^2} - \frac{\partial^2}{\partial x_i x_j}(\rho u_i u_j + P_{ij}) = \frac{\partial}{\partial t}\left[\rho_0 v_n \delta(f)\right] - \frac{\partial}{\partial x_i}\left[l_i \delta(f)\right]. \tag{2.8}$$

Similar to the procedure of the derivation of Lighthill's equation, if we now write $p' = c_0^2 \rho'$ and subtract $\nabla^2 p'$ from eq. (2.8), we get the Ffowcs Willams-Hawkings (FW-H) equation [12] as

$$\frac{1}{c_0^2}\frac{\partial^2 p'}{\partial t^2} - \nabla^2 p' = \frac{\partial}{\partial t}\left[\rho_0 v_n \delta(f)\right] - \frac{\partial}{\partial x_i}\left[l_i \delta(f)\right] + \frac{\partial^2}{\partial x_i x_j}\left[T_{ij} H(f)\right] \tag{2.9}$$

where $H(f)$ is the Heaviside function of f. The three terms on the right-hand side of the FW-H equation, eq. (2.9), are known as the thickness, loading and quadrupole source terms. The FW-H equation generalizes Lighthill's equation. The thickness and loading terms arise from surface contributions whereas the quadrupole term arises from volume contributions to the sources.

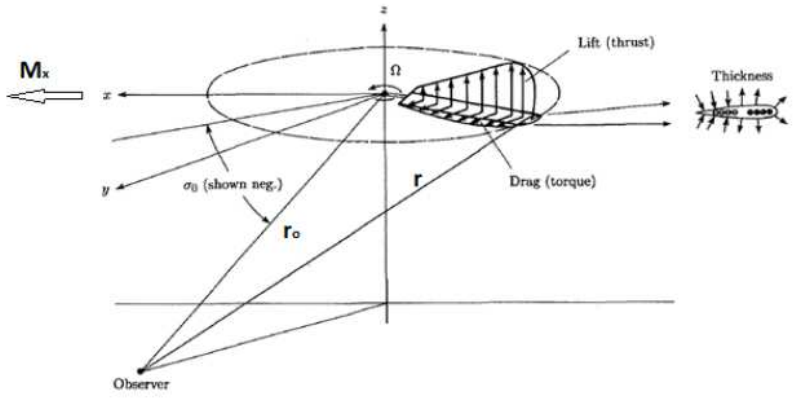

FIGURE 1. Surface forces and geometric description of a single rotor blade.

3. Asymptotic Methods for Propeller Noise

The FW-H equation is valid through the entire space so that its solution can be written in terms of the Green's function of the wave equation as

$$p' = -\int_{-\infty}^{\infty}\int_{S(\tau)}\left(\rho_0\, v_n\,\frac{\partial G}{\partial \tau} + l_i\,\frac{\partial G}{\partial y_i}\right) dS(y)d\tau + \int_{-\infty}^{\infty}\int_{V(\tau)} T_{ij}\,\frac{\partial G}{\partial y_i\, y_j}\, dV(y)d\tau \tag{3.1}$$

where the Lighthill stress tensor components T_{ij} become

$$T_{ij} = \rho u_i u_j + (p' - c_0^2\,\rho')\,\delta_{ij} \tag{3.2}$$

for inviscid flow and where the Green's function of the wave equation for the entire space is given by

$$G(\mathbf{x},t;\mathbf{y},\tau) = \frac{\delta(t-\tau-r/c_0)}{4\,\pi\, r} \tag{3.3}$$

for $-\infty < \tau \leq t$ and zero for $\tau > t$ with $r = |\mathbf{x}-\mathbf{y}|$, $(\mathbf{x},t)$ and $(\mathbf{y},\tau)$ denoting the observer and source space-time coordinates.

Most of the applications of the FW-H equation has been for rotating sound fields, in particular, for propeller noise. In this case the FW-H equation can be solved in two different domains: time domain and frequency domain. Time-domain methods are used to solve eq. (2.9) directly in terms of the space-time variables. These methods are appealing because they can treat blade geometry with any desired level of precision without any approximation [1]. However, in the time domain, singularities will occur as the Mach number of the source in the direction of the observer approaches unity. For this reason, many workers (i.e. Hawkings and Lowson [13] and Hanson [18]) have taken the step of Fourier transforming the equation into the frequency domain. Moreover, they employed the thin blade approximation so that the surface integrals could be replaced by integrating over the mean planform area. The thin blade approximation also leads to the dropping of the quadrupole term in the original equation (2.9). In applying frequency domain methods to the FW-H equation, some precision in the representation of blade geometry is usually lost through the transformation, but this loss is generally acceptable for harmonics to a fairly high order. The transformation also gives rise to Bessel functions which are indicators of radiation efficiency [18]. Harmonics are computed once at a time and waveforms are generated by summing a Fourier series. A transformation to the frequency domain eliminates the need for computing retarded blade locations and their numerical derivatives. By representing blades as helicoidal surfaces, far-field noise formulas that are easily coded on a personal computer can be derived. Furthermore, these formulas give direct insight to the influence of blade geometry and operating conditions on the sound harmonics.

Parry and Crighton [45] carried out the analytical evaluation of the Hanson integrals by asymptotics for steady loading dipole and monopole thickness noise of a propeller. In the case of straight blade, the phase contribution due to blade sweep is set equal to zero, because chordwise noncompactness factors are not important for low and moderate subsonic speeds. With these assumptions, Hanson's integral for subsonic speeds can be

written in the harmonic components of the sound field as [45]

$$p' \;=\; -\,\frac{\rho_0\, c_0^2\, D\, B}{8\,\pi\, r_0\,(1\;-\;M_x\, cos\theta)}$$

$$\times \sum_{m=-\infty}^{\infty} exp\Big[\,\frac{imB\,\Omega}{1\;-\;M_x\, cos\theta}\,\Big(\,t\;-\,\frac{r_0}{c_0}\,\Big)\;+\;i\,m\,B\,\Big(\,\frac{\pi}{2}\;-\psi_0\,\Big)\,\Big]\;P_m \tag{3.4}$$

where m is the harmonic number, B is the number of blades, r_0 is the distance between the observer and the propeller hub, Ω is the propeller shaft angular speed, θ is the radiation angle between the propeller axis and the observer point, ψ_0 is the circumferential angle and M_x is the forward flight Mach number (see Figure 1). In eq. (3.4), P_m is mth harmonic component of the sound field and is given by

$$P_m \;=\; \int_{s_0}^{1} S_m(s)\, J_{mB}\Big[\,\frac{m\,B\,s\,M_t\, sin\theta}{(1\;-\;M_x\, cos\theta)}\Big]\; ds \tag{3.5}$$

where J_n denotes Bessel function of the first kind and of order n, s is the normalized chordwise coordinate of the blade with unity at the blade tip and M_t is the blade tip Mach number. The source strength $S_m(s)$ in eq. (3.5) is

$$S_m(s) \;=\; M_r^2\,\Big(\,i\,k_y\,\frac{C_L}{2}\,\Big) \tag{3.6}$$

for loading and

$$S_m(s) \;=\; M_r^2\,\Big(\,k_x^2\,\frac{b}{c}\,\Big) \tag{3.7}$$

for thickness where M_r is the relative Mach number of the blade section,C_L is the lift coefficient of the blade, b the maximum blade thickness, c is the chordwise blade length, and where the wave numbers k_x and k_y are given by

$$k_x \;=\; \frac{2\,m\,B\,(c/D)\,M_t}{M_r\,(1\;-\;M_x\, cos\theta)}\,, \tag{3.8}$$

$$k_y \;=\; \frac{2\,m\,B\,(c/D)\,(M_r^2\, cos\theta\;-\;M_x}{s\,M_r\,(1\;-\;M_x\, cos\theta)}\,. \tag{3.9}$$

If the order of the Bessel function mB in eq. (3.5) is assumed to be large, the Debye approximation [52] holds:

$$J_{mB}(sech\beta) \;=\; \frac{exp[m\,B\,(tanh\beta\;-\;\beta)\,]}{(2\,\pi\,m\,B\,tanh\beta)^{1/2}} \tag{3.10}$$

where β is given by

$$sech(\beta) \;=\; \frac{s\,M_t\, sin\theta}{1\;-\;M_x\, cos\theta}\,. \tag{3.11}$$

With the Debye approximation, eq. (3.5) becomes

$$P_m \;=\; \int_{s_0}^{1} S_m(s)\;\frac{exp[m\,B\,(tanh\beta\;-\;\beta)\,]}{(2\,\pi\,m\,B\,tanh\beta)^{1/2}}\; ds \tag{3.12}$$

with β given by eq. (3.11). Equation (3.12), in the limit $m\,B\;\rightarrow\;\infty$ suggests the use of Laplace's method [48,49] for the evaluation of integrals containing an exponential term with large argument, where the major contribution to the integral arises from the blade tip ($s = 1$). This integral, to first order, was first carried out by Parry and Crighton [45], where the term $S_m(s)$ in eq. (3.12) was approximated by a power law for both loading and

thickness. In this work we generalize this by using a polynomial fit for $S_m(s)$ for loading in the form

$$S_m(s) \;=\; \sum_{\ell=0}^{N} (S_m)_\ell \, (1 \,-\, s)^\ell \,, \tag{3.13}$$

and retaining the power law dependence for thickness in the form

$$S_m(s) \;=\; \bar{S} \, (1 \,-\, s)^\nu \,. \tag{3.14}$$

The first order asymptotic formulas of Parry and Crighton [45] for subsonic flow in the far field become

$$P_m \;=\; \frac{exp[m\,B\,(tanh\beta_t \,-\, \beta_t)\,]}{(2\,\pi\,m\,B\,tanh\beta_t)^{1/2}} \sum_{\ell=0}^{N} (S_m)_\ell \, \frac{\Gamma(\ell \,+\, 1)}{(m\,B\,tanh\beta_t)^{\ell+1}} \tag{3.15}$$

for loading and

$$P_m \;=\; \frac{exp[m\,B\,(tanh\beta_t \,-\, \beta_t)\,]}{(2\,\pi\,m\,B\,tanh\beta_t)^{1/2}} \, \bar{S} \, \frac{\Gamma(\nu \,+\, 1)}{(m\,B\,tanh\beta_t)^{\nu+1}} \tag{3.16}$$

for thickness where β_t is β evaluated at the blade tip ($s = 1$). Second order integrals for loading and thickness are also given by Zafer et al. [46,47] using Laplace's method. For the same source functions $S_m(s)$, the second order asymptotic formulas become

$$P_m \;=\; \frac{exp[m\,B\,(tanh\beta_t \,-\, \beta_t)\,]}{(2\,\pi\,m\,B\,tanh\beta_t)^{1/2}} \sum_{\ell=0}^{N} (S_m)_\ell \, \frac{\Gamma(\ell \,+\, 1)}{(m\,B\,tanh\beta_t)^{\ell+1}} \times \alpha^{\ell+1} \, D_{-\ell-1}(\alpha) \, exp\Big[\, \frac{\alpha^2}{4} \,\Big] \tag{3.17}$$

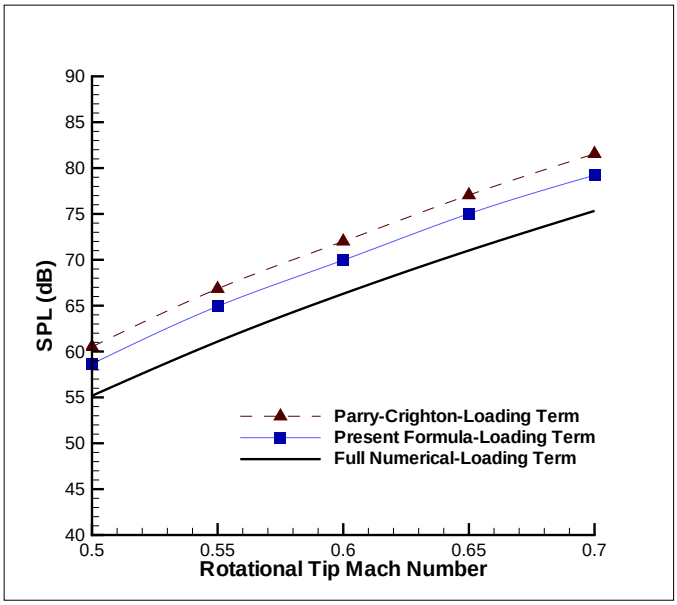

FIGURE 2. Comparison of asymptotic predictions for the loading term between the Parry-Crighton formula [45], and the present formula (eq. 3.17) [46,47] and full numerical solution [53] for the SPL (dB) for an observer located at $r_o = 100$ m with a radiation angle $\theta = 60^o$.

for loading and

$$P_m \;=\; \frac{exp[m\,B\,(tanh\beta_t \,-\, \beta_t)\,]}{(2\,\pi\,m\,B\,tanh\beta_t)^{1/2}}\;\bar{S}\;\frac{\Gamma(\nu\,+\,1)}{(m\,B\,tanh\beta_t)^{\nu+1}}\;\alpha^{\nu+1}\,D_{-\nu-1}(\alpha)\,exp\Big[\,\frac{\alpha^2}{4}\,\Big] \tag{3.18}$$

for thickness where $D_{-\nu}(x)$ is Whittaker's parabolic cylinder function [51] and where α is given by

$$\alpha \;=\; \frac{m\,B\,tanh\beta_t}{\sqrt{2\,m\,B\,\kappa^2\,(cosh^3\beta_t/sinh\beta_t)}} \tag{3.19}$$

with κ defined by

$$\kappa \;=\; \frac{M_t\,sin\theta}{1\;-\;M_x\,cos\theta}\,. \tag{3.20}$$

We can now compare the first and second order asymptotic formulas obtained with full numerical solution of the loading and thickness noise terms. For the full numerical solution of the loading and thickness noise of the helicopter rotor, the integrals given by eq. (3.5) for the mth harmonic pressure P_m should be carried out and should be summed over all harmonics. Therefore, an accurate numerical scheme is needed where the high order Bessel functions are evaluated within any desired accuracy. Fortunately a very fast algorithm for the evaluation of high order Bessel functions already exists [53]. This algorithm is useful since it does not require recalculations using the normalization relations. Instead, it uses the continued fractions method to evaluate the ratio of J_n/J_{n-1} for a sufficiently large value of n. Using Gaussian quadrature together with the above mentioned algorithm for high order Bessel functions, the full numerical solution of the radiation integrals for loading

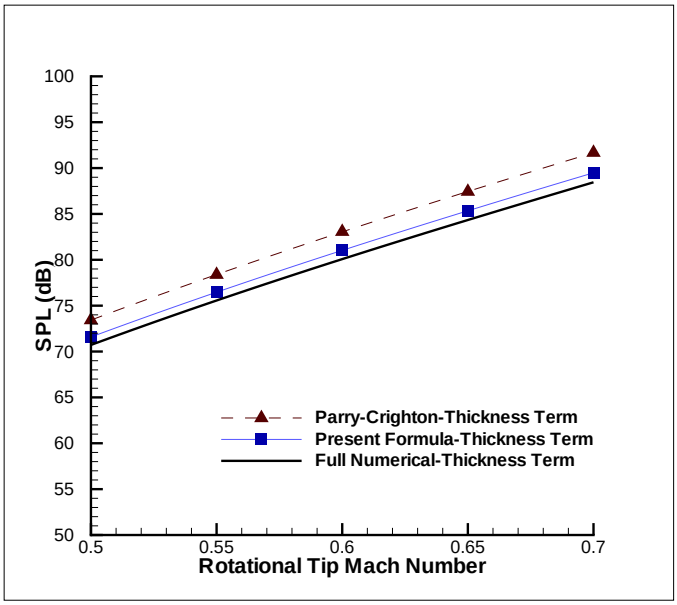

FIGURE 3. Comparison of asymptotic predictions for the thickness term between the Parry-Crighton formula [45], and the present formula (eq. 3.18) [46,47] and full numerical solution [53] for the SPL (dB) for an observer located at $r_o = 100$ m with a radiation angle $\theta = 60^o$.

and thickness noise of the rotor blades can be obtained within any desired accuracy. The aerodynamic loading for the rotor are obtained by CFD computations independently. As a result of this computation [46], the calculated pressure, lift and drag coefficients (C_p, C_L and C_D) are taken as input to the aeroacoustic computation, both in asymptotics and in full numerical computations. For the aerodynamic computations, a three dimensional body fitted computational grid is generated for a rectangular rotor blade with SC1095 airfoil section. The grids that are used here have 121 points in the wraparound direction, 43 points in the normal direction and 31 points in the spanwise direction (121x43x31). The grid was clustered near the leading and trailing edge and also near the tip region. Finite volume method is used to calculate the flow field by using ROE discretization scheme with the Spalart-Allmaras turbulence model. The 3D compressible CFD code first validated against the results of Wake and Baeder [54] for a four bladed helicopter rotor in hover. In this case, the tip Mach number was chosen in the range between 0.5 and 0.7 and the radiation angle was varied from 0^o to 90^o. Results of the SPL noise for loading and thickness contributions using first and second order asymptotic formulas as well as full numerical results are shown in Figures 2-5. The asymptotic predictions are in better agreement with the full numerical results for thickness than for loading, with the second order asymptotic yielding results very close to the full numerical results in this case. In general, the second order asymptotic is in much better agreement than the first order in comparison with the full numerical computations. This investigation has demonstrated

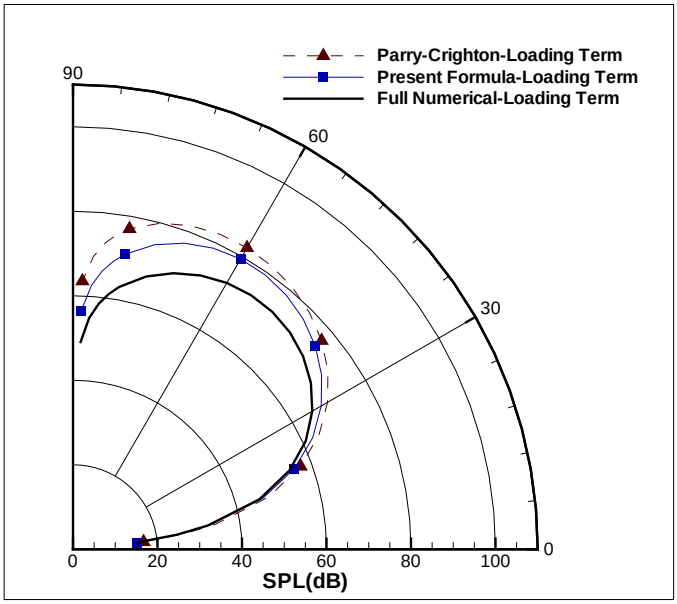

FIGURE 4. Comparison of the Parry-Crighton formula [45] and the present formula [46,47] asymptotic predictions with full numerical computations [53] of the SPL (dB) polar distribution of the loading term with radiation angle $\theta = 60^o$ between 0^o and 90^o from a 4-bladed helicopter rotor in hover at an observer distance $r_o = 100$ m away from the rotor hub and with a tip Mach number (a) $M_t = 0.5$ and (b) $M_t = 0.7$.

the advantages of using the second order asymptotic formulas for loading and thickness, at least for the prediction of the SPL noise of a helicopter rotor in hover in the far field.

4. Computational Aeroacoustics (CAA)

Computational Aeroacoustics (CAA) can be considered as a branch of applied mathematics. The basic idea is replacing the governing differential equation of fluid flow with a set of algebraic equations. This process is called discretization. All of the discretizated equations can be solved with the aid of a digital computer to get an approximate solution. The well-known discretization methods used in CFD / CAA are Finite Difference Method (FDM), Finite Volume Method (FVM), Finite Element Method (FEM) and Boundary Element Method (BEM). The best choise of numerical discretization requires computational efficiency, easy implementation of boundary conditions, efficiency of parallelization, memory usage and proper numerical capability in complex geometries and flow configurations. All numerical discretization methods have advantages as well as disadvantages [42]. In CAA, optimized high order finite difference schemes are used because of the required high resolution and high accuracy.

Finite difference method (FDM) is the oldest (Euler, 1834) method used in the numerical solution of differential equations. Here the domain including the boundary of the physical problem is covered by a grid or mesh. At each of the interior grid points, the original differential equations are replaced by equivalent finite difference approximations. For first

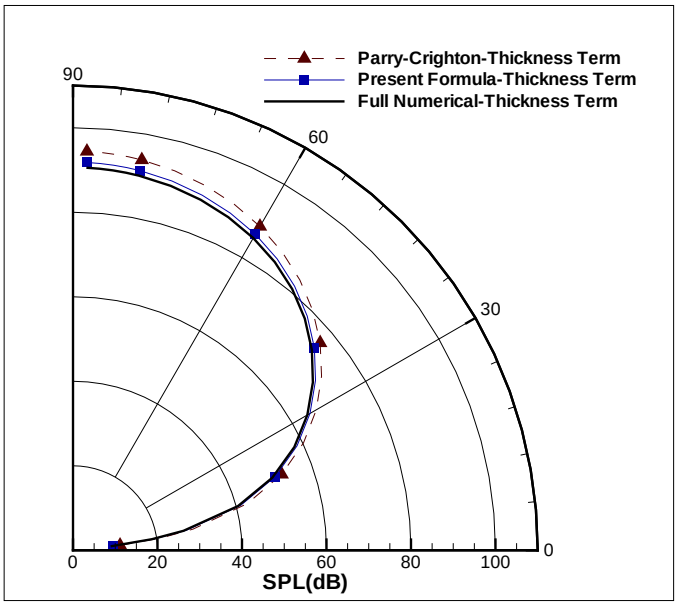

Figure 5. Comparison of the Parry-Crighton formula [45] and the present formula [46,47] asymptotic predictions with full numerical computations [53] of the SPL (dB) polar distribution of the loading term with radiation angle $\theta = 60^o$ between 0^o and 90^o from a 4-bladed helicopter rotor in hover at an observer distance $r_o = 100$ m away from the rotor hub and with a tip Mach number (a) $M_t = 0.5$ and (b) $M_t = 0.7$.

order differential equations, the generic form of any finite difference scheme for a function $f(x)$ with first derivative $f'(x)$ can be written as

$$\sum_{j=-L}^{L} \beta_j \, f'_{\ell+j} \;=\; \frac{1}{\Delta x} \sum_{j=-M}^{N} a_j \, f_{\ell+j} \;+\; O(\,[\Delta x]^n\,) \quad \ell \;=\; 1, 2, ..., m\,. \tag{4.1}$$

where m is the number of grid points. In eq. (4.1), $f_\ell \;=\; f(x_\ell)$, $f'_\ell \;=\; f'(x_\ell)$, M and N denote, respectively, the number of grid points used in the finite difference formula to the left and to the right of the point x_ℓ, $a_j \;;\; j = -M, ..., N$ are the coefficients relating the values of the function f at the neighboring grid points of any finite difference formula and $\beta_j \;;\; j = -L, ..., L$ with $\beta_0 = 1$ are the coefficients relating the values of the first order derivative f' at the neighboring grid points of the implicit finite difference formula. If $L = 0$, the scheme is termed explicit. By contrast, if $L \neq 0$, then it is called implicit or compact. In compact finite difference schemes, each derivative depends on the value of its neighboring derivatives. Therefore, it requires the solution of a linear system of equations to determine the values of the derivatives. On the contrary, the values of each derivative are independent of its neighbors in explicit finite difference schemes. Conventionally, the coefficients are chosen to give the largest possible exponent, n, in the error term. In the Taylor series expansions of the generic equation (4.1), the maximum possible exponent is given by

$$n_{max} \;=\; 2\,L \;+\; M \;+\; N\,. \tag{4.2}$$

The error term is a function of the order of accuracy of the scheme. The leading order term in the truncation error in eq. (4.1), depends on choice of coefficients and the order of the highest derivative truncated in the Taylor series expansion. It is a good measure of the actual error only for sufficiently small Δx when high order derivatives of the function are continuous [55]. To provide a more useful estimate of the magnitude of the error, we refer to the work of Lele [31] and Tam and Webb [30] In addition, it is possible to optimize the coefficients of finite difference schemes to reduce dissipation and dispersion errors. In what follows we discuss the frequently used high order schemes for CAA, namely the Dispersion Relation Preserving scheme and the Optimized Compact scheme.

4.1. **High Order Schemes for CAA.** Dispersion Relation Preserving (DRP) finite difference scheme was proposed by Tam and Webb [30] used to discretize the governing differential equations. They used central difference, i.e., $N = M$, for spatial discretization. The discretization of any DRP scheme for the spatial partial derivative on a uniform grid with spacing Δx can be written as

$$\left(\frac{\partial f}{\partial x} \right)_\ell \;=\; \frac{1}{\Delta x} \sum_{j=-M}^{N} a_j^{MN} \, f_{\ell+j}\,. \tag{4.3}$$

where a_j^{MN}'s are the coefficients optimized to reduce the error within any required order of accuracy and ℓ is an integer representing the grid nodes. The notation of the coefficients a_j^{MN} represents a stencil of width $N \;+\; M \;+ 1$ for computing the spatial partial derivative of a function using the values of the function starting at M points to the left and ending at N points to the right of the node (x_ℓ) where the derivative is evaluated. In particular, the case $N = M$ corresponds to central difference stencils, the case of $N \neq M$ corresponds to non-central difference stencils and the case of either $M = 0$ or $N = 0$

corresponds to the one-sided difference stencils. Traditionally, the stencil coefficients a_j^{MN} are found by expanding the right side of eq. (4.3) as Taylor series in Δx and then equating coefficients of the same powers of Δx. This truncated Taylor series method does not offer any information on propagation errors when the finite difference approximation is used to solve wave propagation problems. Tam and Webb [30] considered the finite difference approximation using Fourier analysis. In their approach, Δx was taken of finite size, not necessarily small. They regarded the coefficients a_j^{MN} to be free parameters that were to be determined so that eq. (4.3) was an optimized approximation. Typical coefficients for a 7-point central difference stencil ($N = M = 3$) for which $a_{-j}^{33} = -a_j^{33}$ are shown in Table 1.

TABLE 1. The DRP scheme coefficients of Tam and Webb [30] for a 7-point stencil ($N = M = 3$) where $a_{-j}^{33} = -a_j^{33}$; $j = -1, -2, -3, 0$.

j	-3	-2	-1	0
a_j^{33}	-0.0208431427703	0.166705904415	-0.770882380518	0.0

The Pade type or compact finite difference schemes are different from the explicit schemes. One of the important difference between the two schemes is that the compact schemes approximate derivatives implicitly where the derivatives are solved for. Another difference is that the compact schemes use less stencil points and have smaller dispersion errors compared to explicit schemes of the same order of accuracy. Higher computational costs is the disadvantage of compact schemes since extra efforts are needed to solve the linear system that contains all the derivatives. Lele [31] showed the spectral-like resolution of the compact schemes for the evaluation of spatial derivatives. The emphasis was on improving a wide range of wave numbers rather than simply increasing the order of accuracy. A family of compact schemes was derived by matching the Taylor series coefficients of various orders. The first unmatched coefficient was the formal truncation error of the scheme. Here, in addition to the DRP scheme discussed above, we also use the Optimized Compact (OC) scheme of Kim and Lee [33]. This scheme is constructed from the equation

$$\beta \left(\frac{\partial f}{\partial x} \right)_{\ell-2} + \alpha \left(\frac{\partial f}{\partial x} \right)_{\ell-1} + \left(\frac{\partial f}{\partial x} \right)_{\ell} + \alpha \left(\frac{\partial f}{\partial x} \right)_{\ell+1} + \beta \left(\frac{\partial f}{\partial x} \right)_{\ell+2}$$

$$= \frac{1}{\Delta x} \sum_{j=1}^{3} a_j \left(f_{\ell+j} - f_{\ell-j} \right) \quad \ell = 1, 2, ..., m \,. \tag{4.4}$$

where f_ℓ and $(\partial f/\partial x]_\ell$, respectively, denote the values of the function and its spatial partial derivative at a grig point x_ℓ, Δx denotes the spacing in a uniform grid, a_j ; $j = 1, 2, 3$ are the coefficients of discretization and where α and β are the coefficients of the compact scheme. Matching the same terms from the Taylor series expansion of eq. (4.4) up to fourth-order results in the following two equations:

$$1 + 2(\alpha + \beta) = 2 \sum_{j=1}^{3} j \, a_j \tag{4.5}$$

and

$$3\,(\alpha + 2^2\,\beta) = \sum_{j=1}^{3} j^3\,a_j \tag{4.6}$$

By solving the equations obtained by error optimization together with the linear algebraic equations (4.5) and (4.6), all of the five coefficients are determined with maximum resolution among the fourth-order schemes [33]. The optimized coefficients of the Optimized Compact (OC) scheme are shown in Table 2.

TABLE 2. The OC scheme coefficients of Kim and Lee [33].

α	β	a_1	a_2	a_3
0.58627	0.095495	0.643141	0.258601	0.007141

4.2. **One-Dimensional Non-reflecting Boundary Conditions.** For purposes of efficiency and accuracy, appropriate non-reflecting boundary conditions are required for relatively small computational domains. In this case, Hedstrom's classical method of characteristic solution [56] gives the artificial boundary conditions. The main idea of this method is to locally decouple the three waves, namely the entropy wave and the two acoustic waves, and identify them as incoming and outgoing waves. Then the non-reflecting boundary conditions can be obtained by simply setting the characteristic variables, corresponding to incoming characteristic curves, to a constant in time. Thompson [51] has improved Hedstrom's method taking into account the contributions from the time derivatives of the incoming waves. Thompson's approach is intrinsically one-dimensional and is suited for flow perpendicularly reaching the outer boundaries. Giles [57] has generalized Thompson's approach for the case of oblique incidences. In this investigation we will be using Thompson's non-reflecting boundary condition, which we will refer to as the standard boundary condition, together with a new non-reflecting boundary condition (random non-reflecting boundary condition) given below for comparison reasons

Here we introduce a novel non-reflecting boundary condition for one-dimensional unsteady flows based on imposing small random perturbations on the specified boundary conditions to avoid spurious reflections in the artificial computational domain. These small perturbations are produced by a random number generator, and they are implemented in such a way that they alternate in sign in successive time steps. The magnitude of these small perturbations is usually chosen depending on the desired accuracy of the numerical scheme. For the implementation of non-reflecting random boundary conditions in one-dimensional computational domains, we let the specified boundary conditions for the acoustic density, the acoustic flow speed and the acoustic pressure at any boundary point be given by the functions $\rho'(t)$, $u'(t)$ and $p'(t)$, respectively. We also define the numerically calculated values of the acoustic pressure at time t_n, with n denoting the nth time step, by p'^n . The specified value, for sufficiently large n, may deviate considerably from the calculated value if accumulated waves reflect from the boundary into the computational domain. To avoid this, we define a random number RN produced by a random number

generator ($0 \leq RN \leq 1$). We also define an intermediate acoustic pressure p^{*n} at time t_n by

$$p^{*n} \;=\; \big[\,1 \,-\, (RN)\,\big]\, p'(t_n) \;+\; (RN)\, p'(t_{n+1})\,. \tag{4.7}$$

We let ϵ be a very small positive number compared to unity. We can now introduce the non-reflecting random boundary condition for the calculated value p'^{n+1} of the acoustic pressure at t_{n+1} as

$$p'^{n+1} \;=\; p'(t_{n+1}) \;+\; (-1)^n\, \epsilon\, p^{*\,n}\,. \tag{4.8}$$

Similar non-reflecting boundary conditions apply to the acoustic density and to the acoustic flow speed.

4.3. **Application to Transonic Nozzle Flow with Backward Acoustic Disturbance.** As an application of the foregoing CAA schemes, we consider the problem of superimposing a very small amplitude acoustic wave at the exit on the steady isentropic flow of a perfect gas in a quasi-one-dimensional convergent-divergent nozzle and determine its propagation. The governing equations for quasi-one-dimensional nozzle flows can be written as

$$\frac{\partial \rho}{\partial t} \;+\; \frac{1}{A}\,\frac{\partial}{\partial x}\,(\rho u A) \;=\; 0\,, \tag{4.9}$$

$$\rho\Big(\,\frac{\partial u}{\partial t} \;+\; u\,\frac{\partial u}{\partial x}\,\Big) \;+\; \frac{\partial p}{\partial x} \;=\; 0\,, \tag{4.10}$$

$$A\,\frac{\partial p}{\partial t} \;+\; \frac{\partial (p\,u\,A)}{\partial x} \;+\; (\gamma \,-\, 1)\,p\,\frac{\partial (u\,A)}{\partial x} \;=\; 0 \tag{4.11}$$

where ρ, u and p are, respectively, the density, the flow speed and the pressure normalized as

$$\rho \;=\; \frac{\rho_{dim}}{\rho_\infty}\,, \quad u \;=\; \frac{u_{dim}}{a_\infty}\,, \quad p \;=\; \frac{p_{dim}}{\rho_\infty\, a_\infty^2} \tag{4.12}$$

with ρ_∞ and a_∞ denoting, respectively, the density and the isentropic speed of sound in the uniform incoming region of the nozzle and γ denoting the isentropic exponent. In the governing flow equations (4.9)-(4.11), x, t and A, respectively, denote the normalized axial coordinate, the normalized time and the normalized area, and are given by

$$x \;=\; \frac{x_{dim}}{L}\,, \quad t \;=\; \frac{L}{a_\infty}\,, \quad A \;=\; \frac{A_{dim}}{A_{in}} \tag{4.13}$$

with L denoting the characteristic length (e.g., the nozzle entrance height) and A_{in} denoting the nozzle entrance area. In the normalization eqs. (4.12) and (4.13), subscript dim refers to dimensional variables. The system of eqs. (4.9)-(4.11) should be supplemented by appropriate initial and boundary conditions for given nozzle area $A(x)$. In this work we use the following nozzle cross-section area suggested by NASA[50]:

$$A(x) \;=\; \begin{cases} 0.536572 \,-\, 0.198086\, exp[-ln2\left(\frac{x}{0.6}\right)^2] & \text{for } x \geq 0 \\ 1.0 \,-\, 0.661514\, exp[-ln2\left(\frac{x}{0.6}\right)^2] & \text{for } x \geq 0 \end{cases} \tag{4.14}$$

We now consider transonic flow in the nozzle where the Mach number becomes close to unity at the throat. We investigate the problem of determining the effect of upstream

propagation of small amplitude acoustic waves in a steady-state transonic flow in the nozzle, whose geometric configuration is shown in Figure 6. We can then write the normalized unsteady transonic nozzle flow solution in the form

$$\rho(x,t) \;=\; \bar{\rho}(x) \,+\, \rho'(x,t)\,, \tag{4.15}$$

$$u(x,t) \;=\; \bar{u}(x) \,+\, u'(x,t)\,, \tag{4.16}$$

$$p(x,t) \;=\; \bar{p}(x) \,+\, p'(x,t) \tag{4.17}$$

where $(\bar{})$ variables denote the classical steady-state isentropic transonic nozzle flow solution and the $(')$ variables denote the small acoustic perturbations ($\rho' \ll \bar{\rho}$, $u' \ll \bar{u}$ and $p' \ll \bar{p}$). Substituting from eqs. (4.15)-(4.17) into the normalized quasi-one-dimensional transonic nozzle flow equations (4.9)-(4.11), we obtain the following linear system of equations for the acoustic field :

$$\frac{\partial \rho'}{\partial t} \,+\, \bar{u}\,\frac{\partial \rho'}{\partial x} \,+\, \frac{\partial \bar{\rho}}{\partial x}\,u' \,+\, \frac{\partial \bar{u}}{\partial x}\,\rho' \,+\, \bar{\rho}\,\frac{\partial u'}{\partial x} \,+\, \Big(\bar{\rho}\,u' \,+\, \bar{u}\,\rho'\Big)\,\frac{1}{A}\,\frac{dA}{dx} \;=\; 0\,, \tag{4.18}$$

$$\bar{\rho}\Big(\frac{\partial u'}{\partial t} \,+\, \bar{u}\,\frac{\partial u'}{\partial x}\Big) \,+\, \Big(\bar{\rho}\,u' \,+\, \bar{u}\,\rho'\Big)\,\frac{\partial \bar{u}}{\partial x} \,+\, \frac{\partial p'}{\partial x} \;=\; 0\,, \tag{4.19}$$

$$\frac{\partial p'}{\partial t} \,+\, \bar{u}\,\frac{\partial p'}{\partial x} \,+\, \frac{\partial \bar{p}}{\partial x}\,u' \,+\, \gamma\,\frac{\partial \bar{u}}{\partial x}\,p' \,+\, \gamma\,\bar{p}\,\frac{\partial u'}{\partial x} \,+\, \gamma\,\Big(\bar{p}\,u' \,+\, \bar{u}\,p'\Big)\,\frac{1}{A}\,\frac{dA}{dx} \;=\; 0 \tag{4.20}$$

where all $(\bar{})$ variables denote the steady-state solution. We now let the acoustic field be in the form

$$\begin{pmatrix} \rho' \\ u' \\ p' \end{pmatrix} \;=\; Re\,\begin{pmatrix} \hat{\rho}(x) \\ \hat{u}(x) \\ \hat{p}(x) \end{pmatrix}\,e^{i\,\omega\,t} \tag{4.21}$$

where Re denotes the real part of the proceeding expression and ω is the normalized angular frequency of the acoustic field. Substitution of eq. (4.21) into the above system of eqs. (4.18)-(4.19) yield the following linear system of first order ordinary differential equations for the local amplitudes ($\hat{\rho}$, $\hat{u}$, $\hat{p}$).

$$i\,\omega\,\hat{\rho} \,+\, \bar{u}\,\frac{d\hat{\rho}}{dx} \,+\, \frac{d\bar{\rho}}{dx}\,\hat{u} \,+\, \frac{d\bar{u}}{dx}\,\hat{\rho} \,+\, \bar{\rho}\,\frac{d\hat{u}}{dx} \,+\, \Big(\bar{\rho}\,\hat{u} \,+\, \bar{u}\,\hat{\rho}\Big)\,\frac{1}{A}\,\frac{dA}{dx} \;=\; 0\,, \tag{4.22}$$

$$i\,\omega\,\bar{\rho}\,\hat{u} \,+\, \bar{\rho}\,\bar{u}\,\frac{d\hat{u}}{dx} \,+\, \Big(\bar{\rho}\,\hat{u} \,+\, \bar{u}\,\hat{\rho}\Big)\,\frac{d\bar{u}}{dx} \,+\, \frac{d\hat{p}}{dx} \;=\; 0\,, \tag{4.23}$$

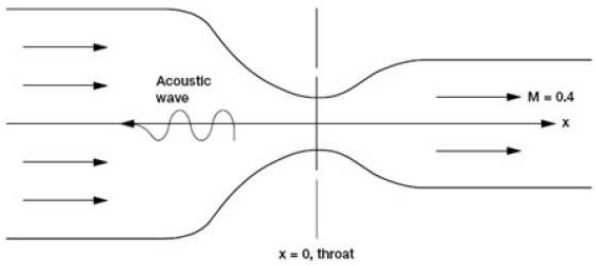

FIGURE 6. The nozzle geometry for acoustic wave interactions in transonic flows.

$$i\,\omega\,\hat{p} \;+\; \bar{u}\,\frac{d\hat{p}}{dx} \;+\; \frac{d\bar{p}}{dx}\,\hat{u} \;+\; \gamma\,\frac{d\bar{u}}{dx}\,\hat{p} \;+\; \gamma\,\bar{p}\,\frac{d\hat{u}}{dx} \;+\; \gamma\left(\bar{p}\,\hat{u} \;+\; \bar{u}\,\hat{p}\right)\frac{1}{A}\,\frac{dA}{dx} \;=\; 0\,. \qquad (4.24)$$

For the classical steady-state solution, we specify the inlet conditions in such a way that we have

$$\bar{\rho}_e \;=\; \bar{\rho}(x_e) \;=\; 1.0\,, \qquad \bar{u}_e \;=\; \bar{u}(x_e) \;=\; 0.4\,, \qquad \bar{\rho}_e \;=\; \bar{\rho}(x_e) \;=\; 1.0/\gamma \qquad (4.25)$$

at the exit where subscript e refers to nozzle exit conditions. The steady state solution corresponding to the boundary conditions specified at the nozzle exit for the cross-sectional area given by eq. (4.14) is obtained using 1600 point uniform mesh points. The normalized density, normalized flow speed (Mach number) and the normalized pressure distributions of such a steady-state isentropic transonic nozzle flow solution of air ($\gamma \;=\; 1.4$) are shown in Figure 7. As can clearly be seen, the flow variables change drastically near the throat region.

We now consider the boundary condition for the acoustic field at the nozzle exit. We let the upstream propagating acoustic disturbance wave at the exit downstream of the nozzle throat be represented by

$$\begin{pmatrix} \rho'_e(t) \\ u'_e(t) \\ p'_e(t) \end{pmatrix} \;=\; \epsilon \begin{pmatrix} 1 \\ -1 \\ 1 \end{pmatrix} cos\Big[\,\omega\,\Big(\frac{x_e}{1\,-\,M_e} \;+\; t\Big)\Big] \qquad (4.26)$$

where x_e is the location of the nozzle exit, M_e is the nozzle exit Mach number, $\epsilon \;=\; 10^{-5}$ and $\omega \;=\; 0.6\,\pi$. The propagation of the acoustic disturbance wave, expressed by eq.(4.26), and its reflection at the nozzle throat can be computed within any desired accuracy by solving the linear system of first order ordinary differential equations subject to the boundary conditions. This solution will be called the exact solution. For uniform region where there is no area change ($dA/dx \;=\; 0$), the exact solution reduces to an

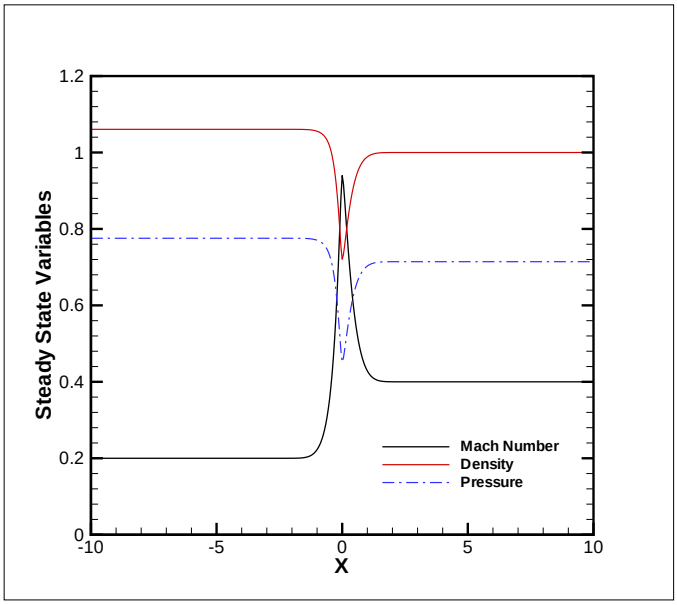

FIGURE 7. The steady-state density, Mach number and pressure distributions in transonic nozzle flow of air for the boundary conditions specified by eq. (4.25).

upstream propagating acoustic wave written as

$$\begin{pmatrix} \hat{\rho}(x) \\ \hat{u}(x) \\ \hat{p}(x) \end{pmatrix} = \begin{pmatrix} \frac{1}{\bar{a}^2} \\ -\frac{1}{\bar{\rho}\,\bar{a}} \\ 1 \end{pmatrix} exp\left[\frac{i\,x}{(\bar{u}\,-\,\bar{a})}\right], \tag{4.27}$$

to a downstream propagating acoustic wave written as

$$\begin{pmatrix} \hat{\rho}(x) \\ \hat{u}(x) \\ \hat{p}(x) \end{pmatrix} = \begin{pmatrix} \frac{1}{\bar{a}^2} \\ \frac{1}{\bar{\rho}\,\bar{a}} \\ 1 \end{pmatrix} exp\left[\frac{-i\,x}{(\bar{u}\,+\,\bar{a})}\right] \tag{4.28}$$

and to an entropy wave written as

$$\begin{pmatrix} \hat{\rho}(x) \\ \hat{u}(x) \\ \hat{p}(x) \end{pmatrix} = \begin{pmatrix} 1 \\ 0 \\ 0 \end{pmatrix} exp\left(\frac{-\,i\,x}{\bar{u}}\right) \tag{4.29}$$

where $\bar{a}$, defined by $\bar{a}^2 = \gamma\,\bar{p}/\bar{\rho}$, is the local frozen isentropic speed of sound. The quasi-one-dimensional transonic nozzle flow with acoustic disturbance discussed above using semi-analytical methods can also be solved by the methods of CAA. For this reason the quasi-one-dimensional transonic nozzle flow equations (4.9)-(4.11) can be expressed in conservative form as

$$\frac{\partial U}{\partial t} + \frac{\partial F}{\partial x} + \frac{1}{A}\frac{dA}{dx}S = 0 \tag{4.30}$$

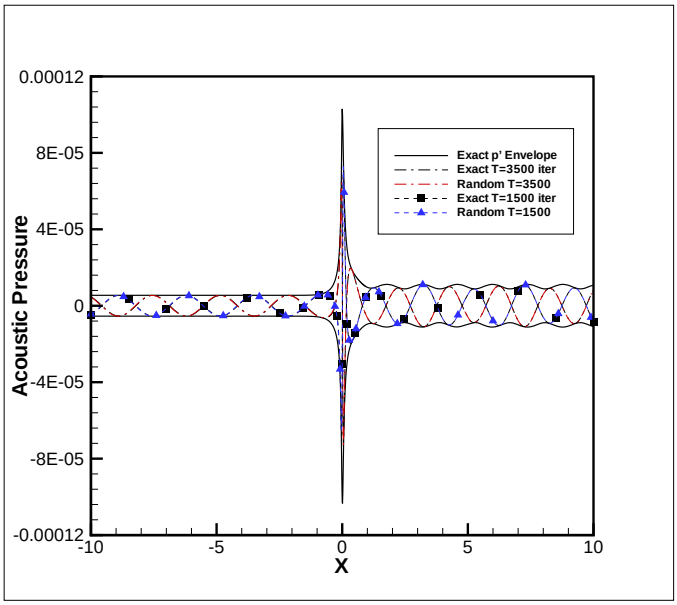

FIGURE 8. The acoustic pressure distributions at different time intervals and their envelope characterizing the maximum acoustic distributions along the nozzle axis in different schemes and non-reflecting boundary conditions.

where the column vectors U, F and S are given by

$$U = \begin{pmatrix} \rho \\ \rho\, u \\ e \end{pmatrix} \quad , \quad F = \begin{pmatrix} \rho\, u \\ \rho\, u^2 + p \\ u\,(e + p) \end{pmatrix} \quad , \quad S = \begin{pmatrix} \rho\, u \\ \rho\, u^2 \\ u\,(e + p) \end{pmatrix}. \tag{4.31}$$

with e defined by $e = p/(\gamma - 1) + (1/2)\,\rho\, u^2$. For the initial field of the above conservation equations, we use the above computed quasi-one-dimensional steady state nozzle flow solution shown in Figure 7. The acoustic wave propagation is then simulated by implanting the acoustic disturbance, given by eq.(4.26), downstream of nozzle. For the discretization of the conservation equations, we use high order schemes, namely the Dispersion-Relation-Preserving (DRP) scheme of Tam and Webb [30] and Optimized Compact (OC) scheme of Kim and Lee [33], both discussed above in some detail. The upstream propagating acoustic disturbances will partly be reflected from the area of the transonic nozzle throat and partly transmitted to the upstream of the nozzle throat. At the nozzle throat, the sound wave amplitude will be amplified. Therefore, to ensure that the computed solutions are of high quality on the computational domain, non-reflecting boundary conditions has to be imposed on both sides of the computation domain. Accurate boundary condition implementations are important for successful simulations of flows with acoustic perturbations. For transonic nozzle flow, the inflow boundary conditions should accurately specify the inflow conditions and the outflow boundary conditions must allow the outgoing perturbations to pass without introducing non-physical reflections back into the computational domain. For this reason two different non-reflecting boundary conditions are used. One of them is the well-known standard non-reflecting boundary condition of Thompson [51],

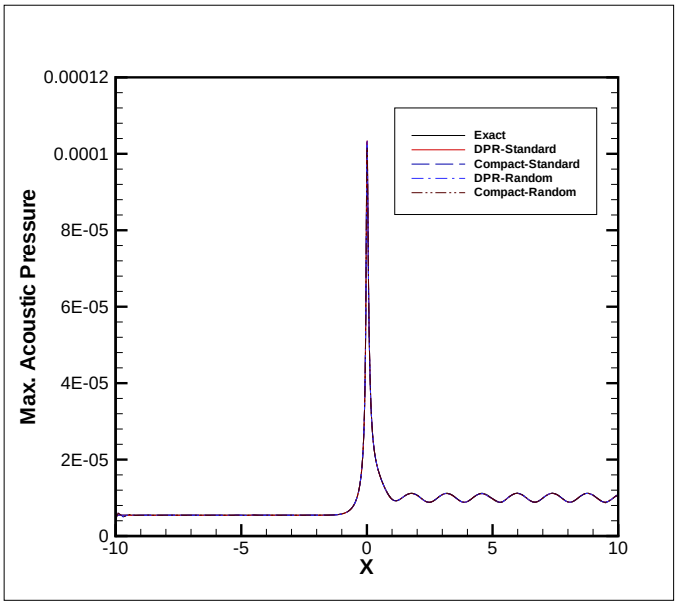

FIGURE 9. Comparison of the maximum acoustic distributions along the nozzle axis in DRP and Optimized Compact (OC) schemes for standard and random non-reflecting boundary conditions.

which is based on the solution of the linearized Euler equations by the method of characteristics. The second one is a novel non-reflecting boundary condition, herein called the random non-reflecting boundary condition, which uses an intermediate value of the acoustic perturbations at the boundary weighted by a random number. Both non-reflecting boundary conditions are discussed above in some detail and are implemented in the two computational aeroacoustic schemes used (DRP and OC). Another important issue is to obtain an accurate solution by using as few grid points as possible. Therefore, a nonuniform grid must be taken into account. For this reason Erickson grid stretching function [58] is used and optimized to transform the x-coordinate. The grid study optimization reduces the number of grid points to a minimum of 250 grid points for an accurate solution, as compared to the exact solution obtained from the linearized perturbation equations.

Figure 8 shows the exact acoustic pressure distributions at two different times of the period, corresponding to phase shifts of $3\,\pi/4$ and $7\,\pi/4$. Also plotted is their envelope, hereafter called *the maximum acoustic pressure*. The results of the DRS-scheme and the OC-scheme agree exceptionally well with the exact solution of the perturbation equations no matter whether the standard non-reflecting boundary condition [51] or the present random boundary condition is employed. The maximum acoustic pressure along the entire computational domain and its detailed structure in the exit region are plotted in Figs. 9 and 10, respectively. The agreement seems excellent for both schemes using two different non-reflecting boundary conditions, especially demonstrating the validity of the random non-reflection introduced in this study.

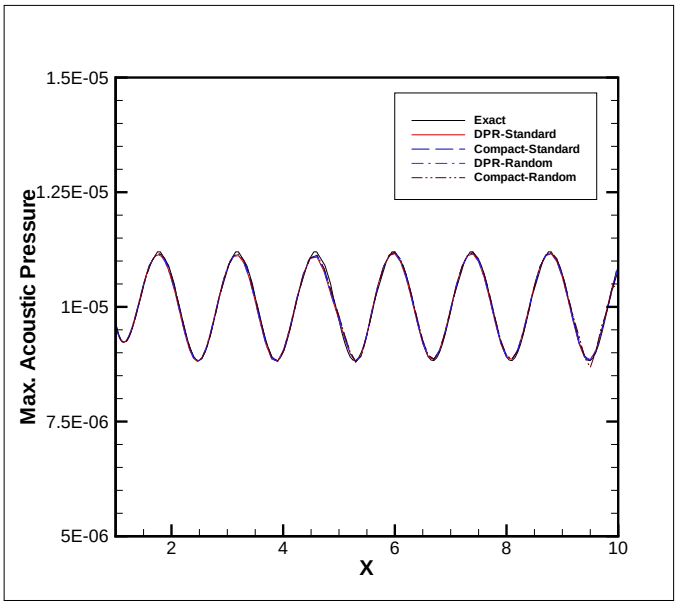

FIGURE 10. Detailed comparison of the maximum acoustic distributions in different schemes and non-reflecting boundary conditions at the exit region of the nozzle.

5. Conclusions

In this paper two different aeroacoustic problems are investigated. In the first problem, propeller noise is investigated using the Green's function solution of the FW-H equation. This equation generalizes Lighthill's acoustic analogy taking into account the contributions from surface source distributions. In this case the source terms can be characterized as monopole, dipole and quadrupole sources, which are, respectively, called thickness, loading and volumetric noise. In this investigation we neglect the quadrupole term and use the frequency domain solution given by Hanson[18] using helicoidal coordinates to represent the thickness and loading source terms for subsonic flow. What results is an integral formula which is applied to investigate helicopter blade noise by asymptotic methods [45-47]. In particular, we investigate the first and second order asymptotic predictions of Hanson's integral formula, as well as the full numerical computations, for the thickness and loading noise of a subsonic B-bladed helicopter rotor. We obtain the first and second order asymptotic formulas using the Debye approximation for Bessel functions of high order and evaluating the resulting integral by Laplace's method [48,49]. In addition, full numerical solution of Hanson's integral is found by using fractional series for Bessel function in the case of large argument and large order and numerical integrals are carried out by Gaussian quadrature [53]. A 3D compressible CFD code is used to compute the aerodynamic loading on the straight rectangular blade of a 4-bladed helicopter rotor in hover. For this case, the blade tip Mach number is chosen in the range between 0.5 and 0.7 so that the flow field remains subsonic. The aerodynamic loading data is fitted by a polynomial of second degree to obtain the loading source term in Hanson's integral. The SPL noise is then calculated by the first and second order asymptotic formulas and by full numerical computations taking into account the loading and thickness contributions. The differences in the SPL noise seem to increase with increasing Mach number, with the second order asymptotics being in much better agreement than the first order in comparison with the full numerical computations. This investigation has demonstrated the advantages of using the second order asymptotic expression for loading and thickness, at least for the prediction of the SPL noise of a helicopter rotor in hover in the far field.

In the second problem, the capabilities of the implementation of high order computational aeroacoustic schemes are investigated for a NASA benchmark problem. In this problem the effect of acoustic wave propagation in transonic nozzle flow is investigated by solving the unsteady quasi-one-dimensional transonic nozzle equations in conservative form, where high order computational accuracy is required. For the initial distribution we use the classical quasi-one-dimensional steady-state nozzle flow solution. The acoustic disturbance is implemented at the nozzle exit and is reflected from the nozzle throat. Therefore, for a valid solution, a high order computational scheme with acceptable resolution is required. For this reason we use high order finite difference computational aeroacoustic schemes, namely the Dispersion Relation Preserving (DRP) scheme of Tam and Webb [30] and the Optimized Compact scheme (OC) of Kim and Lee [33]. Both schemes use central difference, but in the vicinity of the inflow and outflow boundaries, they require non-centered difference scheme. In the latter case the coefficients of the non-centered differences are optimized in the same way as for the interior points. In addition,

the implemented boundary conditions must be avoid reflecting small acoustic perturbations back into the computational domain. For this reason two different non-reflecting boundary conditions are used. One of them is the well-known standard non-reflecting boundary condition of Thompson [51], which is based on the solution of the linearized Euler equations by the method of characteristics. The second one is a novel non-reflecting boundary condition, herein called random non-reflecting boundary condition, which uses an intermediate value of the acoustic perturbations at the boundary weighted by a random number. Both non-reflecting boundary conditions are implemented in the two computational aeroacoustic schemes used (DRP and OC). The numerical results obtained for each scheme are then compared against those obtained by the exact solution of the unsteady quasi-one-dimensional linearized nozzle flow equations. In particular, the exact and computed maximum pressure envelope and time-dependent pressure distributions show very good agreement.

Acknowledgements

Part of this work was completed in partial fulfillment of the PhD Thesis of Mr. Baha Zafer at Istanbul Technical University.

References

[1] Brentner, K. S., (1994), Helicopter Noise Prediction: The Current Status and Future Direction, J. Sound Vibration, 170, 79-96.
[2] Gutin, L., (1936), On the sound field of a rotating propeller, Zh. Tekh. Fiz., 6, 899-909.
[3] Ernsthausen, W., (1936), The source of propeller noise, Luftfahrtforschung, 8, 433-440.
[4] Deming, A. F., (1938), Noise from propellers with symmetrical sections at zero blade angle II, NACA TM, 679.
[5] Garrick, I. E., (1954), A theoretical study of the effect of forward speed on the free-space sound-pressure field around propellers, NACA Report, 1198.
[6] Arnoldi, R. A., (1956), Propeller noise caused by blade thickness, Unite Aircraft Corporation Research Department Report, R-896.
[7] Lighthill, M. J., (1952), On sound generated aerodynamically. I. General theory, Proc. Roy. Soc. London A, 211, 564-587.
[8] Farassat, F., (1981), Linear Acoustic Formulas for Calculation of Rotating Blade Noise, AIAA J., 19, 1122-1130.
[9] Lowson, M. V., (1965), The sound field for singularities in motion, Proc. Roy. Soc. London A, 286, 559-572.
[10] Wright, S. E., (1969), Sound radiation from a lifting rotor generated by asymmetric disk loading, J. Sound Vibration, 9, 223-226.
[11] Lowson, M. V. and Ollerhead, J. B., (1969), A theoretical study of helicopter rotor noise, J. Sound Vibration, 9, 197-222.
[12] Ffowcs Williams, J. E. and Hawkings, D. L., (1969), Sound Generation by Turbulence and Surfaces in Arbitrary Motion, Roy. Soc. London-Philosophical Trans. A, 264, 321-342.
[13] Hawkings, D. L. and Lowson, M. V., (1974), Theory of open supersonic rotor noise, J. of Sound and Vibration, 36, 1-20.
[14] Farassat, F., (1977), A new capability for predicting helicopter rotor and propeller noise including the effect of forward motion, NASA TM, X-74037.
[15] Farassat, F., (1975), Thickness noise of helicopter rotors at high tip speeds, AIAA Paper 75-453.
[16] Yu, Y. H., (1978), The influence of the transonic flow field on high-speed helicopter impulsive noise, Fourth European Rotorcraft and Powered Lift Aircraft Forum.

[17] Hanson, D. B., (1976), Near field noise of high tip speed propellers in forward flight, AIAA Paper 76-565.
[18] Hanson, D. B., (1980), Helicoidal Surface Theory for Harmonic Noise of Propellers in the Far Field, AIAA J., **18**, 1213-1220.
[19] Leverton, J. W., (1989), Twenty-five years of rotorcraft aeroacoustics: Historical prospective and important issues, J. Sound Vibration, 133, 261-287.
[20] Brooks, T. F., (1989), Main rotor broadband noise study in the DNW, J. Am. Heli. Soc., 34, 3-12.
[21] Martin, R. M., (1988), Acoustic results of the blade-vortex interaction acoustic test of a 40 percent model rotor in the DNW, J. Am. Heli. Soc., 33, 37-46.
[22] Farassat, F., (1983), The prediction of helicopter rotor discrete frequency noise, Vertica, 7, 309-320.
[23] Brentner, K. S., (1986), Prediction of helicopter discrete frequency roto"r noise - A computer program incorporating realistic blade motions and advanced acoustic formulation, NASA TM, 87721.
[24] Lyrintzis, A. S., (1994), Review: The use of Kirchhoff's method in computational aeroacoustics, J. Fluids Eng., 116, 665-676.
[25] Brentner, K. S., (1998), Analytical comparison of the acoustic analogy and Kirchhoff formulation for moving surfaces, AIAA J., 36, 1379-1386.
[26] Brentner, K. S. and Farassat, F., (1998), Supersonic quadrupole noise theory for high-speed helicopter rotors, J. Sound Vibration, 218, 481-500.
[27] Howe, M. S., (1999), Trailing edge noise at low Mach numbers, J. Sound Vibration, 225, 211-238.
[28] Ianniello, S., (1999), Quadrupole noise predictions through the Ffowcs Williams-Hawkings equation, AIAA J., 37, 1048-1054.
[29] Ianniello, S., (2001), Aeroacoustic analysis of high tip-speed rotating blades, Aerospace Science and Technology, 5, 179-192.
[30] Tam, C. K. and Webb, J. C., (1993), Dispersion-relation-preserving finite difference schemes for computational acoustics, J. Comp. Phys., 107, 262-281.
[31] Lele, S. K., (1992), Compact finite difference schemes with spectral-like resolution, J. Comp. Phys., 103, 16-42.
[32] Haras, Z. and Taasan, S., (1994), Finite difference schemes for long-time integration, J. Comput. Phys., 114, 265-279.
[33] Kim, J. W. and Lee, D. J., (1996), Optimized compact finite difference schemes with maximum resolution, AIAA J., 34, 887-893.
[34] Hixon, R., (2000), Prefactored small-stencil compact schemes, J. Comp. Phys., 165, 522-541. 35. D. W. Zingg 2001 Comparison of high-accuracy finite-difference methods for linear wave propagation, *SIAM J. Sci. Comp.*, 22, 476-502.
[35] Hixon, R. and Turkel, E., (2000), Compact implicit MacCormack-type schemes with high accuracy, J. Comp. Phys., 158, 51-70.
[36] Zingg, D. W., Lomax, H. and Jurgens, H., (1996), High-Accuracy Finite-Difference Schemes for Linear Wave Propagation, SIAM J. Sci. Comp., 17, 328-346.
[37] Hu, F. Q., Hussaini, M. Y. and Manthey, J. L., (1996), Low-dissipation and low-dispersion Runge-Kutta schemes for computational acoustics, J. Comp. Phys.,124, 177-191.
[38] Stanescu, D. and Habashi, W. G., (1998), 2N-storage low dissipation and dispersion Runge-Kutta schemes for computational acoustics, J. Comput. Phys., 143, 674-681.
[39] Tam, C. K., (1995), Computational aeroacoustics: Issues and methods, AIAA J., 33, 1788-1796, 1995.
[40] Tam, C. K., (2004), Computational Aeroacoustics: An Overview of Computational Challenges and Applications, Int. J. Comp. Fluid Dyn., 18, 547-567.
[41] Colonius, T. and Lele, S. K., (2004), Computational aeroacoustics: Progress on nonlinear problems of sound generation, Prog. Aerospace Sci., 40, 345-416.
[42] Wells, V. L., (1997), Computing aerodynamically generated noise, Ann. Rev. Fluid Mech., 29, 161-199.
[43] Wang, M., Freund, J. B. and Lele, S. K., (2006), Computational Prediction of Flow-Generated Sound, Ann. Rev. Fluid Mech., 38, 483-512.
[44] Parry, A. B. and Crighton, D.C., (1989), Asymptotic theory of propeller noise - Part I: Subsonic single-rotation propeller, AIAA J., 27, 1184-1190.

[45] Zafer, B., Delale, C. F. and Aslan, A. R., (2005), Second order asymptotics for propeller noise and application to helicopter rotor blades, In Proc. Ankara International Aerosapace Conference (AIAC), 127-135.
[46] Zafer, B., Sen, A.L., Delale, C. F. and Aslan, A. R., (2007), Asymptotic prediction and full numerical solution of helicopter rotor noise in the far field, In Proc. Ankara International Aerosapace Conference (AIAC), 87-94.
[47] Erdelyi, A., (1956), Asymptotic expansions, Dover publications, New York.
[48] Hinch, E. J., (1994), Perturbation methods, Cambridge University Press.
[49] Hardin, J. C., Huff, D. and Tam, C. K. W., (2000), Proc. Third Computational Aeroacoustics (CAA) Workshop on Benchmark Problems, NASA/CP-2000-209790.
[50] Thompson, K. W., (1987), Time dependent boundary conditions for hyperbolic systems, J. Comp. Phys., 68, 1-24.
[51] Abramowitz, M. and Stegun, I. A., (1965), Handbook of mathematical functions, Dover Publications, New York.
[52] Ratis, Y. L. and De Cordoba, P. F., (1993), A code to calculate (high order) Bessel functions based on the continued fractions method, Comp. Phys. Com., 76, 381-388.
[53] Wake, B. E. and Baeder, J. D., (1996), Evaluation of a Navier-Stokes analysis method for hover performance prediction, J. Am. Heli. Soc., 41, 7-17.
[54] Hoffman, J. D., (2001), Numerical Methods for Engineers and Scientists, CRC Press.
[55] Hedstrom, G. W., (1979), Nonreflecting boundary conditions for nonlinear hyperbolic systems, J. Comp. Phys., 30, 222-237.
[56] Giles, M. B., (1990), Nonreflecting boundary conditions for Euler equation calculations, AIAA J., 28, 2050-2058.
[57] Erickson, L. E., (1982), Generation of boundary-conforming grids around wing-body configurations using transfinite interpolation, AIAA Journal, 20, 1313-1320.

Can F. Delale worked as Associate and Full Professors at Boğaziçi, Bilkent, Istanbul and Istanbul Technical Universities before he joined Işık University in 2009. He received his BS degree in Mechanical Engineering from ITU, his MS degree in Physics from Lehigh University (USA) and his PhD from Brown University, with major in Thermodynamics and Fluid Mechanics. He also worked abroad as Alexander von Humboldt Fellow at Karlsruhe University of Technology and at Max Planck Institute für Strömungsforschung in 1992 and 1993, as Burgers' Center Research Professor at Eindhoven University of Technology in 1995 and 1996, as Royal Society and British Council Fellow at the University of Cambridge in 1995 and 1998, as invited scientist at California Institute of Technology in 2000 and at the University of Tokyo in 2002 and as a DAAD Fellow at Munich Technical University in 2008. In 1995 he was elected Associate Member of the Turkish Academy of Sciences. His research interests include the kinetic theory of gases, gas/liquid transitions, gas dynamics with condensation, wave phenomena, hydrodynamic cavitation and aeroacoustics.

Baha Zafer was born in Istanbul. In 1997, he attended the Faculty of Aeronautics and Astronautics at Istanbul Technical University (ITU). He graduated from the Astronautics Engineering Department of the same faculty with second rank. In 2002, he worked at the Von Karman Institute of Fluid Dynamics in Belgium during summer time. At the same year, he began Master of Science degree at ITU in the program of Advanced Technologies in Engineering. He was granted the Master of Science degree in 2005. He continued as a PhD student in the same program. Since 2002, he has been a research assistant in the Faculty of Aeronautics and Astronautics. His research interests are computational fluid dynamics, numerical methods and aeroacoustics. He is married.

A. Rüstem Aslan is the head of the Department of Astronautical Engineering at Istanbul Technical University (ITU) since 2004 and is the Deputy Director of Rotorcraft Center of Excellence of ITU since 2003. Dr. Aslan received his BSc and MSc degrees from the ITU Department of Aeronautical Engineering. He completed the Diploma Course of the von Karman Institute for Fluid Dynamics in 1986. He received his Ph.D. from the same institute together with Universite Libre de Bruxelles in 1991. He was a visiting professor at Old Dominion University, USA, between 2001 and 2002. Dr. Aslan's research interests include the design, analysis and development of pico- and nanosatellites, manned and unmanned rotorcraft systems, computational fluid dynamics, fluid mechanics and aerodynamics, and defense and education technologies. Dr. Aslan has authored or co-authored over eighty technical publications. His twenty-six research projects have been sponsored by various civil and military funding agencies and industries.